Available online at www.sciencedirect.com

ScienceDirect

Ceramics International 35 (2009) 653–659

CERAMICS INTERNATIONAL

www.elsevier.com/locate/ceramint

Ionic conductivity and mechanical properties of Y_2O_3-doped CeO_2 ceramics synthesis by microwave-induced combustion

Yen-Pei Fu *

Department of Materials Science and Engineering, National Dong Hwa University, Shou-Feng, Hualien 974, Taiwan

Received 12 November 2007; received in revised form 9 December 2007; accepted 28 January 2008
Available online 29 April 2008

Abstract

We developed a new method, i.e. microwave-induced combustion synthesis to produce highly sinterable Y_2O_3-doped CeO_2 nanopowders. The process took only 15 min to yield Y_2O_3-doped CeO_2 powders. We also investigated the conductivity of Y_2O_3-doped CeO_2 ceramics. It was found Y_2O_3 concentration to have a large effect on the morphology, activation energy, ionic conductivity, and mechanical properties of Y_2O_3-doped CeO_2 ceramics. The results revealed that the bulk densities of Y_2O_3-doped CeO_2 ceramics sintered at 1420 °C for 5 h were all higher than 92% of the theoretical densities, and the maximum ionic conductivity, $\sigma_{800\,^\circ\mathrm{C}} = 0.023$ S/cm at 800 °C, the minimum activation energy, $E_a = 0.954$ eV determined in the temperature of 300–800 °C and the maximum fracture toughness, $K_{IC} = 1.825 \pm 0.188$ MPa m$^{1/2}$ were found for 9 mol.% Y_2O_3-doped CeO_2 specimen. The grain size of CeO_2 decreases with increasing Y_2O_3 concentration. The fracture toughness was found to increase at increased Y_2O_3 concentration, because of the decrease of CeO_2 grain size.

Keywords: A. Microwave processing; C. Hardness; C. Ionic conductivity; D. CeO_2; E. Fuel cells

1. Introduction

Nanopowders have many excellent properties suited for various applications of ceramics such as gas sensors, rechargeable batteries, fuel cells, and so on. In addition, they can significantly enhance sintering rates, decrease sintering temperature, and improve optical, electric, and magnetic properties compared to micrometer size powders [1,2]. As such, solid oxide fuel cells are attracting widespread attention due to their high-energy conversion efficiency and low pollution. The high oxide ionic conducting solid electrolytes based on zirconia have been intensively investigated in the past [3,4]. In order to reduce the operation temperature from 1000 to 800 °C or even lower, doped ceria has been considered as the solid electrolyte for moderate temperature solid oxide fuel cells. Contrary to pure yttria-stabilized zirconia (YSZ), $CeO_{2-\delta}$, has the fluorite structure and oxygen vacancies ($V_O^{\bullet\bullet}$) as the predominant ionic defect [5–7]. The oxygen vacancy concentration and concomitant oxide ion conductivity, in CeO_2 can be increased by the substitution of a lower-valent metal such as Y, Sm, Gd, and Ca. Also, Y_2O_3-doped CeO_2 has been considered as the solid electrolyte for moderate temperature solid oxide fuel cells [8]. However, the ion conductivity of CeO_2 can be significantly improved upon substitution of some trivalent oxides, because the number of oxygen vacancy will be greatly increased for charge compensation. The electrical conductivity in doped ceria is influenced by several factors such as the dopant ion, the dopant concentration, the oxygen vacancy concentration, and the defect association enthalpy. Their relationships are closely and complicatedly related to the electrical conductivity in doped ceria. Such relationship is not simple point to point, but a combined result of several factors. However, besides the global lattice parameter change, localized defect structure and energetics might also have significant influence [9–11].

There are several methods for preparing Y_2O_3-doped CeO_2 nanopowder such as hydrothermal synthesis [12], thermophoresis-assisted vapor phase synthesis [13], and sol–gel techniques [14]. In this research, we have attempted a new method, the microwave-induced combustion synthesis process, to produce Y_2O_3-doped CeO_2 nanopowders and the advantage of this process The advantages of this process are (1) simple process: all the reactions take only a few minutes, not like the other

---

* Tel.: +886 3 863 4209; fax: +886 3 863 4200.
E-mail address: d887503@alumni.nthu.edu.tw.

0272-8842/$34.00 © 2008 Elsevier Ltd and Techna Group S.r.l. All rights reserved.
doi:10.1016/j.ceramint.2008.01.027

methods that require tedious process; (2) simple equipment: this method does not require complicated equipment; (3) cheap sources: chemicals used in this method are cheap, unlike special materials needed in sol–gel process. Moreover, microwave processing of materials is fundamentally different from the conventional processing due to its heating mechanism. In a microwave oven, heat is generated within the sample itself by the interaction of microwaves with the material. In conventional heating, the heat is generated by heating elements, which is then transferred to the sample surfaces. The microwave-induced combustion synthesis process involves the dissolution of nitrates and urea in water, followed by heating the solution in a microwave oven. The urea and metal nitrate decompose and give flammable gases. After the solution reaches the point of spontaneous combustion, it begins burning and results in burning at high temperature. Combustion is not complete until all the flammable substances are consumed, and the resulting material is a loose, highly friable substance exhibiting voids and pores formed by the escaping gases during the combustion reaction [15,16]. The whole process takes only a few minutes to yield Y_2O_3-doped CeO_2 nanopowder. These nanoscale Y_2O_3-doped CeO_2 powders can reduce sintering temperature compared to those powders prepared by solid-state reaction.

Materials used in SOFC system may be susceptible to fracture due to thermal stress and mechanical stress during cell fabrication and operation. Unfortunately, ceria-based materials possess weak mechanical strength. It may conduct ceria-based ceramics their application for electrolyte [17]. The addition of rare earth oxide to CeO_2 can slightly improve its mechanical properties. In current research, we present the results of a systematic study of the structure, mechanical and electrical properties of Y_2O_3-doped CeO_2 ceramics which powders were from microwave-induced combustion process.

2. Experimental procedures

2.1. Sample synthesis

The synthesis process involved the combustion of redox mixtures, in which a metal nitrate acted as an oxidizing reactant and urea as a reducing one. The initial composition of the solution containing cerium nitrate, yttrium nitrate hexahydrate, and urea was based on the total oxidizing and reducing valences of the oxidizer and the fuel using the concepts of the propellant chemistry [18].

Stoichiometric amounts of cerium nitrate ($Ce(NO_3)_3 \cdot 6H_2O$), yttrium nitrate hexahydrate ($Y(NO_3)_3 \cdot 6H_2O$), and urea ($CO(NH_2)_2$) dissolved in a minimum quantity of water, were placed in a crucible. The crucible containing the solution was then introduced into a microwave oven (CEM, MDS 81D, 650 W). Initially, the solution boils and undergoes dehydration followed by decomposition with the evolution of large amount of gases. After the solution reaches the point of spontaneous combustion, it begins burning and releases lots of heat, vaporizes all the solution instantly and becomes a solid burning at high temperature. The powder samples prepared by microwave-induced combustion process were pelletized and sintered at 1420 °C for 5 h. The sintered samples were over 92% of the theoretical density for all specimens.

2.2. Characterization techniques

A computer-interface X-ray powder diffractometer (XRD) with Cu Kα radiation (Rigaku D/Max-II) was used to identify the crystalline phase and determine the crystallite size. The crystallite size D_{XRD} was calculated according to the Scherer equation [19]: $D_{XRD} = 0.9\lambda/B \cos\theta$, where λ is the wavelength of the radiation, θ is the diffraction angle, and B is the corrected half-width of the diffraction peak, give by $B^2 = B_m^2 - B_s^2$, where B_m is the measured half-width of the diffraction peak and B_s is the half-width of standard CeO_2 with a crystal size greater than 100 nm. The reflection from the (1 1 1) plane, occurring at 28.620⊖, was used to calculate the crystallite size. The crystallite size determined from the broadening curve is in the range of 14–17 nm. When using the Scherer equation, we assume that the particle size is the only source of peak broadening; however, if compositional non-uniformity occurs in the particles, the particle size will be underestimated. Differential thermal analysis and thermogravimetry (TG/DTA, Rigaku Thermalplus TG 8120) were used to study the exo-endo temperature of as-received CeO_2 powders. A heating rate of 10 °C/min was used in both the DTA and TG measurements up to 1000 °C in air. BET surface area measurements where made by nitrogen adsorption Micromeritics ASAP 2020 and calculated using the five point Brunauer–Emmit–Teller (BET) theory. Mean particle size (D_{BET}) was calculated from the BET data according to $D_{BET} = 6/(\rho_{th} S_{BET})$, where S_{BET} is the measured surface area and ρ_{th} is the theoretical density of the compound [20]. The morphological features of the particle were examined by transmission electron microscope (TEM, JEOL JEM-200CX) with an accelerating voltage of 200 kV. For sintered specimens, the ionic conductivity was measured by a two-point dc method on a sintered Y_2O_3-doped CeO_2 pellet. Electrodes were formed by applying platinum paste to the two ends of the pellet and firing at 800 °C for 1 h. The ionic conductivity measurements were made at various temperatures in the range of 300–800 °C in air. Arrhenius plots (plots of log σ vs. $10^3/T$) were then constructed and activation energies for conduction were computed. Finally, the densities and porosities of sintered ceramics were measured by the Archimedes method.

Vickers hardness was measured using a microhardness tester (Akashi MVK-H110, Tokyo, Japan) with the load 1000 g, and held for 10 s. At least 10 indentations were used for obtained mean and standard deviation value of hardness and fracture toughness. All specimens were polished with a series of emery paper of 800, 1000, 1200, and 1500 grit. Contamination on the surface was ultrasonically cleaned with ethanol. The Vickers indenter hardness was determined by the average value of both diagonals with a Vickers indenter apex of 136° and calculated with follow equation: $H_V = 1.8544\ P/d^2$ where P is the load, and d is the mean value of both diagonals.

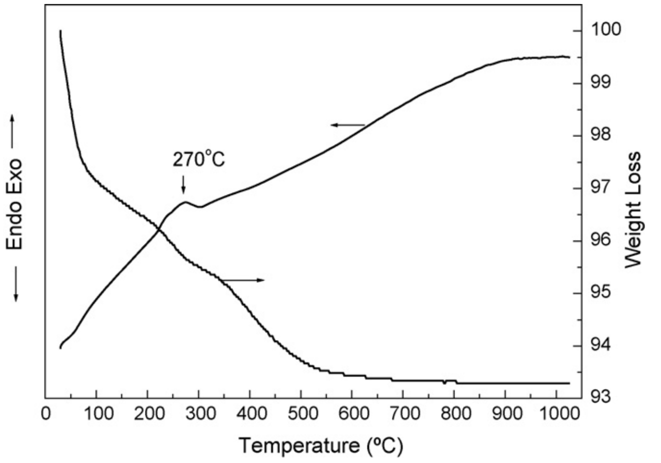

Fig. 1. DTA/TG curves for as-received CeO_2 powder prepared by microwave-induced combustion process.

3. Results and discussion

Phase transformations of the resultant powder were studied by using DTA/TG; Fig. 1 shows the DTA/TG traces for as-received CeO_2 powders prepared by microwave-induced combustion. The rapid weight loss before 100 °C is due to loss of water. From 100 to 500 °C the about 3–4% weight loss in the TG curve may be attributed to the combustion of organic matter. This phenomenon is in good agreement with the DTA curve, which shows one exothermic peak at 270 °C. No weight loss occurs above ~550 °C, which indicates that CeO_2 nanopowders at this stage are formed completely without any impurities including organic matters and un-reacted nitrate. Fig. 2 shows TEM micrographs of the CeO_2 doped with different amounts of Y_2O_3, which is evidence of a very broad particle size distribution and agglomeration of particles. In fact, the average particle size ranges from 20 to 30 nm independent of the amount of yttrium doped. As shown in Fig. 2(d), the electron diffraction patterns of 5 mol.% Y_2O_3-doped CeO_2 powder with ring patterns, revealing poly-crystallinity of individual crystallite and also confirm the formation of the cubic fluorite structure in good agreement with the XRD pattern. Table 1 summarizes the data of BET surface area, particle size, crystallite size, and Ψ value of the Y_2O_3-doped CeO_2 powders. It is well known that $\Psi = D_{BET}/D_{XRD}$ is a factor reflecting the agglomeration extent of the primary crystallites. For Y_2O_3-doped CeO_2 powders, D_{BET} and D_{XRD} values show unobvious discrepancies in various Y_2O_3 concentrations. In comparison with D_{BET} and D_{XRD} values, D_{BET} values are always larger than D_{XRD} values, it is due to slight agglomerates occurred in Y_2O_3-doped CeO_2 powders, leading to N_2 gas cannot completely penetrate agglomerates during BET analysis, moreover, XRD can detect the subgrains within particles. The D_{BET} and D_{XRD} of the powders seem not to depend on yttrium amount. The Ψ values were distributed from 1.38 to 1.65.

The X-ray diffraction patterns of Y_2O_3-doped CeO_2 ceramics were identified by the diffractometer. Fig. 3 shows that the Y_2O_3-doped CeO_2 ceramics contain only the cubic fluorite structure with the space group $Fm3m$ (JCPDS powder diffraction File No. 34-0394). No secondary phases are found in all specimens. According to phase equilibrium diagrams as plotted in Fig. 4, it is found that the binary phase diagram of Y_2O_3–CeO_2 system, the solubility of Y_2O_3 in CeO_2 at 1400 °C is about 18 mol.% [21]. Therefore, the result of X-ray diffraction patterns of Y_2O_3-doped CeO_2 ceramics is consistent with phase diagram. The introduction of Y_2O_3 into CeO_2 can cause a small shift in the ceria peaks, and this shift is indicative of change in the lattice parameter. A distribution of different Y_2O_3 amount within individual particles as well as between particles would lead to distribution of 2θ values. Fig. 5 shows the lattice constant of Y_2O_3-doped CeO_2 powder as a function

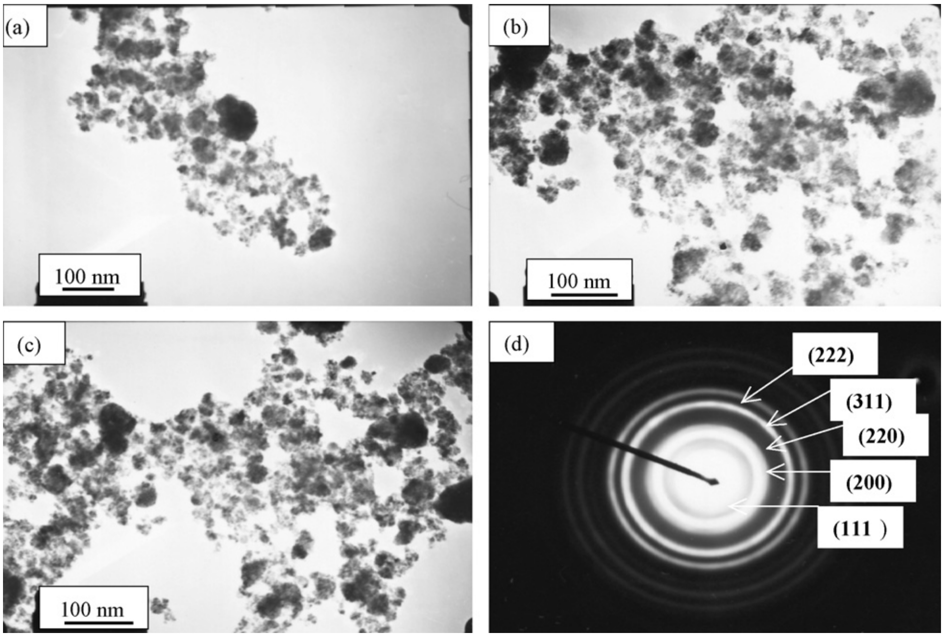

Fig. 2. TEM micrograph of Y_2O_3-doped CeO_2 powders: (a) 1 mol.% Y_2O_3-doped CeO_2, (b) 5 mol.% Y_2O_3-doped CeO_2, (c) 9 mol.% Y_2O_3-doped CeO_2, and (d) electron diffraction pattern of 5 mol.% Y_2O_3-doped CeO_2 powder.

Table 1
Surface area, particle size, and crystallite size of Y_2O_3-doped CeO_2 powders prepared by microwave-induced combustion process

Y_2O_3-doping concentration	Surface area (m^2/g)	Particle size[a] (nm)	Crystallite size[b] (nm)	Ψ[c]
1	37.2 ± 1.2	22.4 ± 0.4	14.6 ± 0.2	1.53 ± 0.03
3	38.6 ± 1.6	21.6 ± 0.3	15.6 ± 0.3	1.38 ± 0.04
5	35.9 ± 1.3	23.2 ± 0.3	15.3 ± 0.2	1.51 ± 0.03
7	33.3 ± 1.1	25.0 ± 0.5	16.4 ± 0.4	1.53 ± 0.04
9	33.7 ± 1.1	24.7 ± 0.4	14.9 ± 0.2	1.65 ± 0.05

[a] Particle size measured from specific surface area.
[b] Crystallite size measured from XRD line broadening.
[c] Ψ = particle size/crystallite size.

of Y_2O_3-doping concentration. The cell parameters were calculated using the four main reflections typical of a fluorite structure material with a fcc cell, corresponding to the (1 1 1), (2 0 0), (2 2 0), and (3 1 1) planes. The lattice parameter (a) of the doped ceria can be calculated by the follow relations:

$$d = \frac{\lambda}{2\sin\theta}; \quad a = d\sqrt{h^2 + k^2 + l^2}$$

where d is the planar spacing, λ is the wavelength of the radiation ($\lambda = 0.15418$ nm), θ is the diffraction angle, a is the lattice parameter. The lattice constant increased with increasing yttrium amount due to the different radii of Ce^{4+} (0.090 nm) and Y^{3+} (0.092 nm) in an oxide solid solution with a fluorite-type structure. Doping Y_2O_3 in a CeO_2 lattice induces uniform strain in the lattice because the material is elastically deformed. This effect causes the lattice plane spacing to change and the diffraction peaks to shift to new 2θ positions. As the Y_2O_3 concentration (mol.%) increases, the lattice constant increases linearly as $a(x) = 5.39774 + 0.00134x$ for Y_2O_3-doped CeO_2 powders (x = 1–9).

Pure CeO_2 ceramics are poor oxide ion conductors. However, the ion conductivity can be significantly improved by increasing the oxygen vacancy concentration by the substitution of yttrium, which is lower than +4 in valence and upon substituting for Ce^{4+} which is charge compensated by an oxygen vacancy. For example,

$$Y_2O_3 \xrightarrow{CeO_2} 2Y''_{ce} + 3O_O{}^x + V_O{}^{\bullet\bullet}$$

In Y_2O_3-doped CeO_2 ceramic, total electrical conductivity is attributed to ionic defect ($V_o{}^{\bullet\bullet}$). The ionic defect population and mobility are sufficiently high, indicating the ionic current overwhelms the electronic. Therefore, the transference number (t_i) is nearly unitary. The ionic conductivities of Y_2O_3-doped CeO_2 ceramics as functions of temperature is plotted in Figs. 6 and 7. The ionic conductivity of Y_2O_3-doped CeO_2 increases

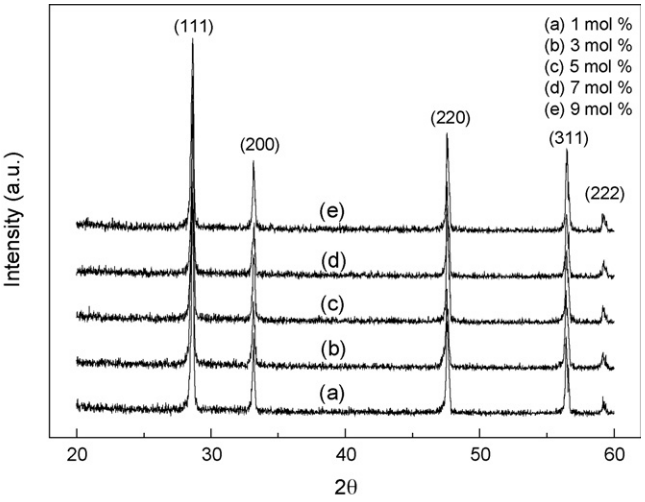

Fig. 3. XRD patterns of Y_2O_3-doped CeO_2 ceramics sintered at 1420 °C for 5 h.

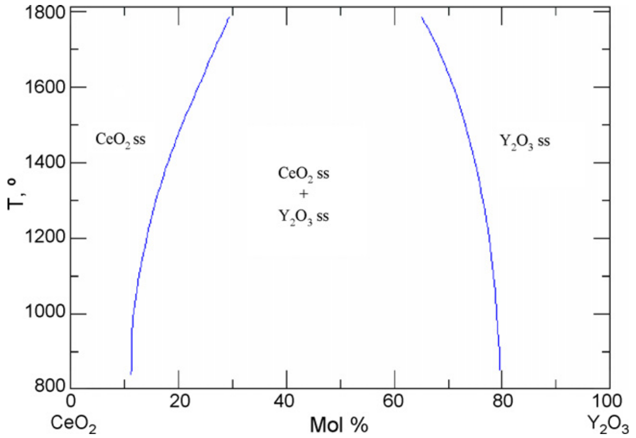

Fig. 4. Phase equilibrium diagram of the system ceria–yttria for temperature between 900 and 1700 °C.

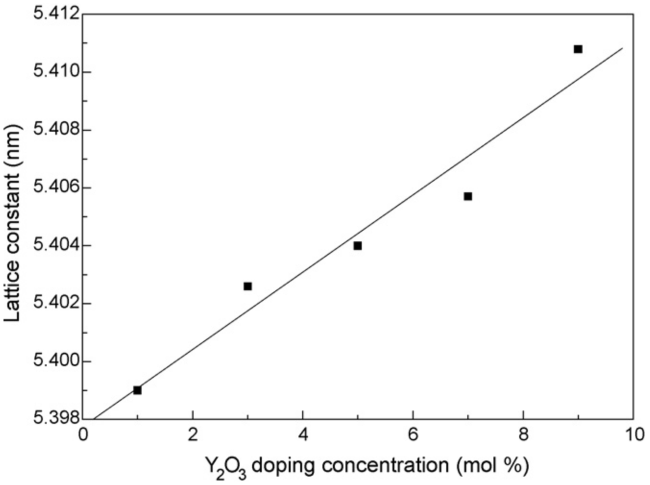

Fig. 5. Lattice constant of Y_2O_3-doped CeO_2 ceramics as a function of Y_2O_3-doping concentration.

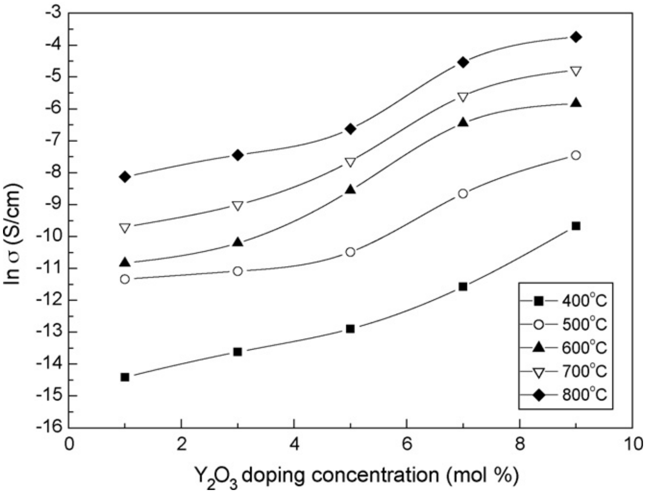

Fig. 6. Y_2O_3-doping concentration dependence of the ionic conductivities of Y_2O_3-doped CeO_2 ceramics at different temperatures.

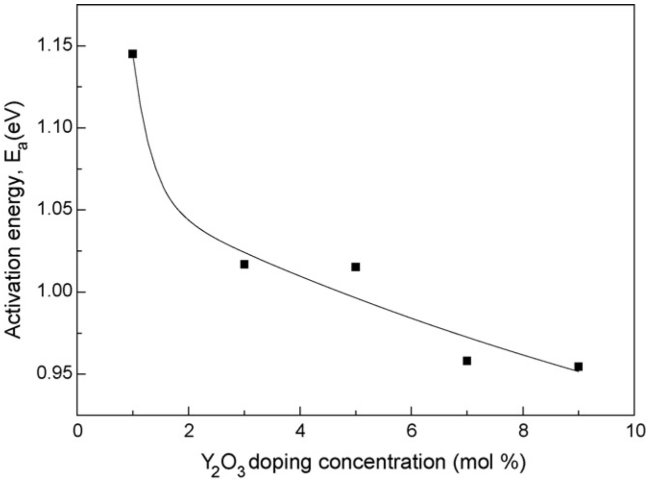

Fig. 8. Variation of the activation energy E_a as a function of Y_2O_3-doping concentration in Y_2O_3-doped CeO_2 ceramics in the temperature range of 300–800 °C.

systematically with increasing Y_2O_3-doping concentration and reaches a maximum for the composition of 9 mol.% Y_2O_3-doped CeO_2 ceramic ($\sigma_{800\ ^\circ C} = 0.023$ S/cm). With increasing temperature, the oxide ion mobility increases and the conductivities increase at high temperatures. Activation energy for conduction is calculated by plotting the ionic conductivity data in the Arrhenius relation for thermally activated conduction. It is calculated according to the following equation: $\sigma_T = \sigma_0 \exp(-E_a/kT)$, where E_a is the activation energy for conduction, T is the absolute temperature, and σ_0 is a pre-exponential factor [22]. Fig. 8 shows the variation of the activation energy E_a as a function of Y_2O_3-doping concentration in Y_2O_3-doped CeO_2 ceramics in the temperature range of 300–800 °C. The activation energy decreases gradually with increasing Y_2O_3-doping concentration and reaches a minimum, $E_a = 0.954$ eV for 9 mol.% Y_2O_3-doped CeO_2 specimen. A summary of relative densities, ionic conductivities, and activation energies of Y_2O_3-doped CeO_2 ceramics sintered at 1420 °C for 5 h is listed in Table 2. It depicts that sintered samples were greater than 92% of the theoretical densities for all specimens. Y_2O_3-doped CeO_2 powders synthesized by microwave-induced combustion process can significantly decrease the sintering temperature, compared with that of the above 1550 °C required for ceria solid electrolysis prepared by solid-state reactions. Y_2O_3 plays an important role in Y_2O_3-doped CeO_2 ceramics, which can provide oxygen vacancies and hinder grain growth in Y_2O_3-doped CeO_2 ceramics, but the oxygen vacancies do not increase without limit. As the solubility limit is reached, is that

Table 2
Relative density, ionic conductivity, and activation energy of Y_2O_3-doped CeO_2 ceramics

Y_2O_3-doping concentration (mol.%)	Relative density (%)	Ionic conductivity (S/cm) at 800 °C	Activation energy (eV) (300–800 °C)
1	92.8	2.94×10^{-4}	1.145
3	93.7	5.81×10^{-4}	1.017
5	94.2	1.32×10^{-3}	1.015
7	95.6	1.07×10^{-2}	0.958
9	95.4	2.37×10^{-2}	0.954

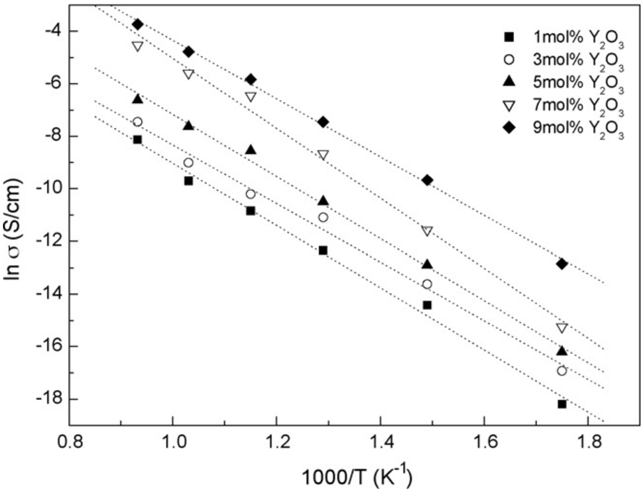

Fig. 7. Arrhenius plots for ionic conductivities of Y_2O_3-doped CeO_2 ceramics.

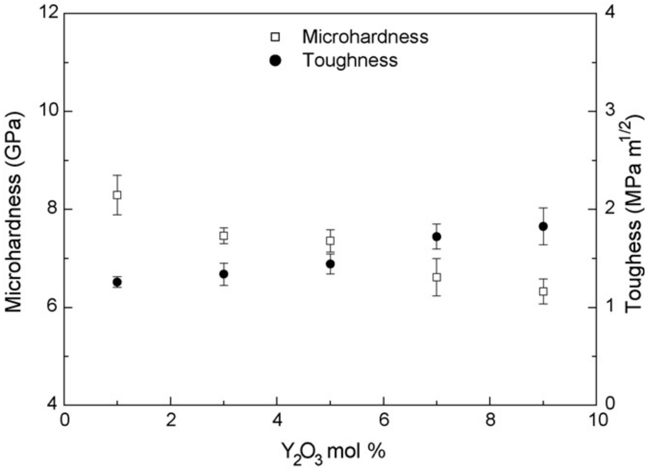

Fig. 9. Fracture toughness and microhardness, respectively, dependent of various Y_2O_3-doping concentration for Y_2O_3-doped CeO_2 ceramics.

Table 3
Fracture toughness and microhardness for Y_2O_3-doped CeO_2 ceramics with various Y_2O_3-doping concentration

Y_2O_3-doping concentration	Microhardness, H_V (GPa)	Fracture toughness, K_{IC} (MPa $m^{1/2}$)
1	8.291 ± 0.403	1.258 ± 0.056
3	7.459 ± 0.163	1.338 ± 0.114
5	7.355 ± 0.227	1.441 ± 0.101
7	6.612 ± 0.381	1.721 ± 0.127
9	6.321 ± 0.252	1.825 ± 0.188

the defect interaction occurred, and then ionic conductivity decreased again at higher Y_2O_3-doping concentration. In this study, 9 mol.% Y_2O_3 has not reached solubility limit for CeO_2–Y_2O_3 system, the defect interaction does not occurred. This phenomenon leads that the ionic conductivity of Y_2O_3-doped CeO_2 increases systematically with increasing Y_2O_3-doping concentration. Oxygen vacancies increase with Y_2O_3-doping concentration under solubility limit for CeO_2–Y_2O_3 system.

Fig. 9 depicted the fracture toughness and microhardness, respectively, vs. Y_2O_3-doping concentration for Y_2O_3-doped CeO_2 ceramics. The fracture toughness vs. crack size was first examined based on the equation as follows [23] (Table 3):

$$K_{IC} = 0.016\left(\frac{E}{H_V}\right)^{1/2}\left(\frac{P}{C^{3/2}}\right)$$

where K_{IC} is fracture toughness, E is Young's modulus, H_V is Vickers hardness, P is the load and C is the half crack size. There are many indentation equations for the calculation of K_{IC} as presented by Ponton and Rawling [24]. There are specific conditions and limitation for using these formulates; so far no universal formula is available to evaluate of K_{IC} for all ceramics materials [25]. For convenience, above-mentioned equation is applied for dealing with the indentation data of doped ceria-based ceramics. There is a decrease in the microhardness with increasing Y_2O_3-doping concentration, and there is an increase in the toughness with increasing Y_2O_3-doping concentration. Since Y_2O_3 may hinder grain growth in CeO_2 ceramics, the grain size decreases with increasing Y_2O_3-doping concentration. This result is in agreement with literature reported that the fracture toughness of Al_2O_3 ceramic decreased with increasing grain size [26]. Pure CeO_2 exhibits a fracture toughness of ~1.5 MPa $m^{1/2}$ [27]. The result revealed that the addition of yttria to CeO_2 can effectively improve the mechanical properties. The fracture toughness was distributed in the range of 1.25–1.82 MPa $m^{1/2}$. When Y_2O_3-doping concentration is greater than 7 mol.%, the fracture toughness is greater than pure CeO_2. The maximum fracture toughness, $K_{IC} = 1.825 \pm 0.188$ MPa $m^{1/2}$ was found in 9 mol.% Y_2O_3-doped CeO_2 ceramic.

4. Conclusions

In this study, using cerium nitrate, yttrium nitrate hexahydrate, and urea as the starting materials, nanoscale Y_2O_3-doped CeO_2 powders have been synthesized successfully by a microwave-induced combustion process. The synthesized Y_2O_3-doped CeO_2 powders with nano-dimension and high specific surface reveal that the particle size ranges from 19 to 25 nm, crystallite size varies from 14 to 16 nm, and the specific surface area is about 33–43 m^2/g. Moreover, the addition of Y_2O_3 amount greatly affects the morphology, ionic conductivity, activation energy, mechanical properties for Y_2O_3-doped CeO_2 ceramics. The experimental results found that the maximum ionic conductivity, $\sigma_{800\,^\circ C} = 0.023$ S/cm at 800 °C, the minimum activation energy, $E_a = 0.954$ eV determined in the temperature of 300–800 °C and the maximum fracture toughness, $K_{IC} = 1.825 \pm 0.188$ MPa $m^{1/2}$ were found in 9 mol.% Y_2O_3-doped CeO_2 specimen.

Acknowledgement

The author would like to thank the National Science Council of Taiwan for financial supporting this research under Contract No. NSC 96-2221-E-259-005.

References

[1] H. Hahn, J. Logas, R. Averback, Sintering characteristics of nanocrystalline TiO_2, J. Mater. Res. 5 (1990) 609–614.

[2] Y.C. Zhou, M.N. Rahaman, Hydrothermal synthesis and sintering of ultrafine CeO_2 powders, J. Mater. Res. 8 (1993) 1680–1686.

[3] E.C. Subbarao, H.S. Maiti, Solid electrolytes with oxygen ion conduction, Solid State Ionics 11 (1984) 317–338.

[4] B.C.H. Steele, Oxygen transport and exchange in oxide ceramics, J. Power Source 49 (1994) 1–14.

[5] H.L. Tuller, A.S. Nowick, Defect structure and electrical properties of nonstoichiometric CeO_2 single crystals, J. Electrochem. Soc. 126 (1979) 209–217.

[6] W. Hung, P. Shuk, M. Greenblatt, Properties of sol–gel prepared $Ce_{1-x}Sm_xO_{2-x/2}$ solid electrolytes, Solid State Ionics 100 (1997) 23–27.

[7] E.K. Chang, R.N. Blumenthal, The nonstoichiometric defect structure and transport properties of CeO_{2-x} in the near-stoichiometric composition range, J. Solid State Chem. 72 (1988) 330–337.

[8] N.Q. Minh, Ceramic fuel cells, J. Am. Ceram. Soc. 76 (3) (1993) 563–588.

[9] H. Inaba, H. Tagawa, Ceria-based solid electrolytes, Solid State Ionics 83 (1996) 1–16.

[10] H. Yahiro, K. Eguchi, H. Arai, Electrical properties and reducibilities of ceria-rare earth oxide system and their application to solid oxide fuel cell, Solid State Ionics 36 (1989) 71–75.

[11] K. Eguchi, T. Setoguchi, T. Inoue, H. Arai, Electrical properties of ceria-based oxides and their application to solid oxide fuel cells, Solid State Ionics 52 (1992) 165–172.

[12] K. Yamashita, K.V. Ramanujachary, M. Greenblatt, Hydrothermal synthesis and low temperature conduction properties of substituted ceria ceramics, Solid State Ionics 81 (1995) 53–60.

[13] W. Bai, K.L. Choy, N.H.J. Stelzer, J. Schoonman, Thermophoresis-assisted vapour phase synthesis of CeO_2 and $Ce_xY_{1-x}O_{2-\delta}$ nanoparticles, Solid State Ionics 116 (1999) 225–228.

[14] X. Luo, B. Zhu, C. Xia, G.A. Niklasson, C.G. Granqvist, Transparent ion-conducting ceria–zirconia films made by sol–gel technology, Sol. Energy Mater. Sol. Cell 53 (1998) 341.

[15] O.A. Lopez, J. McKittrick, L.E. Shea, Fluorescence properties of polycrystalline Tm^{3+}-activated $Y_3Al_5O_{12}$ and Tm^{3+}–Li^+ co-activated $Y_3Al_5O_{12}$ in the visible and near IR ranges, J. Lumin. 71 (1997) 1–11.

[16] Y.P. Fu, C.H. Lin, Preparation of Y_2O_3-doped CeO_2 nanopowders by microwave-induced combustion process, J. Alloys Compd. 389 (1–2) (2005) 165–168.

[17] T. Zhang, Z. Zeng, H. Huang, P. Hing, J. Kliner, Effect of alumina addition on the electrical and mechanical properties of $Ce_{0.8}Gd_{0.2}O_{2-\delta}$ ceramics, Mater. Lett. 57 (2002) 124–129.

[18] S.R. Jain, K.C. Adiga, V.R.P. Verneker, A new approach to thermochemical calculations of condensed fuel-oxidizer mixtures, Combust. Flam. 40 (1981) 71–79.

[19] B.E. Warren, X-Ray Diffraction, Dover Publications, New York, 1990p. 253.

[20] R. Doshi, C.B. Alock, J.J. Carberry, Effect of surface area on CO oxidation by the perovskite catalysts $La_{1-x}Sr_xMO_{3-\delta}$ (M = Co, Cr), Catal. Lett. 18 (1993) 337–343.

[21] V. Longo, L. Podda, Phase equilibrium diagram of the system ceria–yttria for temperature between 900 and 1700 °C, J. Mater. Sci. 16 (1981) 839–841.

[22] C. Tian, S.-W. Chan, Ionic conductivities, sintering temperatures and microstructures of bulk ceramic CeO_2 doped with Y_2O_3, Solid State Ionics 134 (2000) 89–102.

[23] G.R. Anstis, P. Chantikul, B.R. Lawn, D.B. Marshall, A critical evaluation of indentation techniques for measuring fracture toughness. I. Direct crack measurements, J. Am. Ceram. Soc. 64 (1981) 533–538.

[24] B.C. Poton, R.D. Rawling, Vickers indentation fracture toughness test. Part 1. Review of literature and formulation of standard indentation toughness equations, Mater. Sci. Technol. 5 (1989) 865–872.

[25] J. Ma, T.S. Zhang, L.B. Kong, P. Hing, Y.J. Leng, S.H. Chan, Preparation and characterization of dense $Ce_{0.8}Y_{0.15}O_{2-\delta}$ ceramics, J. Eur. Ceram. Soc. 24 (2004) 2641–2648.

[26] T. Tani, Y. Miyamoto, M. Koizumi, M. Shimada, Grain size dependences of Vickers microhardness and fracture toughness in Al_2O_3 and Y_2O_3 ceramics, Ceram. Int. 12 (1986) 33–37.

[27] S. Mashina, O. Shaizero, S. Meriani, Mechanical properties in the ceria–zirconia system, J. Eur. Ceram. Soc. 9 (1992) 127–132.